APPLICATION NOTE
doi.org/10.1002/elsa.202100141

Chemistry Europe
European Chemical Societies Publishing

Received: 31 July 2021
Revised: 23 November 2021
Accepted: 29 November 2021

Vacuum compatible flow-cell for high-quality in situ and operando soft X-ray photon-in–photon-out spectroelectrochemical studies of energy materials

Marc F. Tesch[1] | **Shannon A. Bonke**[2] | **Ronny Golnak**[3] | **Jie Xiao**[3] | **Alexandr N. Simonov**[4] | **Robert Schlögl**[1,5]

[1] Department Heterogeneous Reactions, Max Planck Institute for Chemical Energy Conversion, Mülheim an der Ruhr, Germany
[2] Yusuf Hamied Department of Chemistry, University of Cambridge, Cambridge, UK
[3] Department of Highly Sensitive X-ray Spectroscopy, Helmholtz-Zentrum Berlin für Materialien und Energie GmbH, Berlin, Germany
[4] School of Chemistry and the ARC Centre of Excellence for Electromaterials Science, Monash University, Victoria 3800, Australia
[5] Department Inorganic Chemistry, Fritz Haber Institute of the Max Planck Society, Berlin, Germany

Correspondence
Marc F. Tesch, Max Planck Institute for Chemical Energy Conversion, Department Heterogeneous Reactions, Stiftstraße 34–36, 45470 Mülheim an der Ruhr, Germany.
Email: marc.tesch@cec.mpg.de

Funding information
German Federal Ministry of Education and Research, Grant/Award Number: FKZ 03HY105E; Australian Research Council, Grant/Award Numbers: CE140100012, FT200100317

Abstract

Soft X-ray spectroscopy is a powerful method to investigate materials on an element selective level with respect to their atomic and electronic structure. However, its application is technically challenging for in situ or *operando* investigations of materials for electrochemical applications. Herein, we present a spectroelectrochemical flow-cell designed to enable state-of-the-art electrochemical characterization while being installed in a vacuum chamber for the direct accessibility of the electroactive sample to soft X-rays. An overview of the application of soft X-ray photon-in–photon-out spectroscopic studies to electromaterials is provided, along with discussions of experimental and technical considerations specific to this highly sensitive mode of analysis. Application of the cell for the in situ spectroelectrochemical characterization of an electrodeposited nickel oxide water electrooxidation catalyst is demonstrated.

KEYWORDS
energy materials, flow cell, photon-in–photon-out spectroscopy, soft X-rays, spectroelectrochemistry

1 | INTRODUCTION

The development of materials for energy conversion and storage to facilitate the usage of sustainable energy remains a prominent scientific challenge. Key to guiding this research are developments of in situ and *operando* characterization that allow a deeper understanding of materials under operating conditions.[1–4] This includes spectroscopic work that provides key insights into the nature of active materials, with X-ray spectroscopy being a particularly powerful tool that is sensitive to electronic structure and enables element selective analysis.[5–7] The soft X-ray energy range covers L-edge excitations of 3*d*-transition metals and K-edge excitations of low-Z elements such

as C, N, and O, which are key components of numerous high-performance energy materials and/or of compounds participating in relevant electrochemical processes.

Analysis of materials under electrochemical operating conditions is particularly challenging for photon-in–electron-out techniques such as total electron yield (TEY) and X-ray photoelectron spectroscopy due to the low inelastic mean free path of electrons.[8,9] Photon-in–photon-out spectroscopy, on the other hand, is more flexible due to the higher transmissibility of photons. Several designs of electrochemical flow cells for soft X-ray photon-in–photon-out spectroscopy were reported.[10–14] Such cells are usually based on a single, small-volume electrolyte compartment accommodating all three electrodes, often positioned in an electrochemically imperfect manner. This might compromise the quality of the electrochemical data due to excessively high ohmic losses, inhomogeneous and unknown distribution of the ionic current flow, and interference from the counter electrode processes. The latter aspect is particularly important to continuous experiments involving electrochemically active dissolved species intentionally added and/or generated at the counter electrode during prolonged steady-state measurements required to collect comprehensive X-ray spectroscopic data at a range of potentials. Since the purpose of a spectroelectrochemical experiment is to directly correlate the spectroscopic and electrochemical data, both need to be of high quality and the limitations highlighted above need to be avoided.

Herein we present a vacuum compatible cell for in situ and *operando* soft X-ray photon-in–photon-out spectroelectrochemical studies, that was designed to provide optimized and mutually balanced spectroscopic and electrochemical conditions. This includes a balancing of the electrochemically active and the spectroscopically accessible area, conventional arrangement of the working-reference-counter electrodes, an optimized flow pathway for the electrolyte solution and bubble removal, increased volume (compared to other cells), and spatial separation of the working and counter electrode compartments by an ion conductive polymer separator. Taken together, these and other features of the cell design discussed below avoid instrumental challenges of the electrochemical measurements, while enabling collection of soft X-ray spectroscopic data in situ.

The presented setup is widely applicable to studying electrocatalytic reactions by a variety of techniques including total fluorescence yield (TFY), partial fluorescence yield (PFY), X-ray emission spectroscopy (XES), and resonant inelastic X-ray scattering (RIXS). Its capabilities are demonstrated herein by an in situ TFY study on an electrodeposited NiO_x thin film as an anode material for the oxygen evolution reaction (OER).

2 | TECHNICAL CONSIDERATIONS AND FLOW CELL DESIGN

Soft X-ray spectroscopy of an operating electrode requires a suitable propagation path for the X-rays, as soft X-rays are absorbed by air within several 100 to several 1000 μm at 1 atm and by solids and liquids within several 100 to several 1000 nm.[15] Further, the sample has to be in contact with a conductive support as well as an electrolyte solution. To address these requirements, we designed a vacuum-compatible electrochemical cell (Figure 1) with a focus on providing the best possible electrochemical conditions within a vacuum chamber (see also Section 2 in the Supporting Information).

The flow cell design enables the electrode materials to be selected as required for specific experiments, and typically functions in a conventional three-electrode configuration with a well-defined reference electrode (not a pseudo-reference wire). The working electrode (WE) is a thin conductive layer on an X-ray transparent substrate (further referred to as "membrane") that is typically a free-standing layer of 50–100 nm Si_3N_4 or SiC supported by a Si-frame. A scheme of the X-ray interaction with the sample is depicted in Figure 1c, wherein X-rays approach the working electrode from the vacuum side, and are transmitted through the membrane and WE to interact with the sample in its operative environment. Subsequently, the emitted photons pass back through WE and membrane and travel to the detector. This approach enables a wide variety of electrode materials to be employed, as a material must only be deposited onto the membrane as a sufficiently thin layer for X-ray transmission, for example, using physical vapor deposition. Au is an ideal conductive layer for the WE in many respects due to its inertness, conductivity, and lack of catalytic activity toward many reactions (*cf.* other noble metals). An insertion port allows a reference electrode (RE) to be placed within 1-2 mm of the WE (a "leak-free" Ag|AgCl|KCl system is convenient for aqueous measurements). The counter electrode (CE) is placed into a compartment separated by e.g. a proton conductive polymer, such as Nafion, to avoid interference of dissolved material or products generated at the CE with the processes of interest occurring at the WE. This compartment provides sufficient space to hold a coiled wire or mesh and ensure the surface area of the CE is larger than the WE, as required for stable operation.

The main body of the cell is PEEK to provide exceptionally broad chemical stability. The WE and CE chambers are *ca* 1 and 2 mL in volume, respectively, with the small volumes limiting the risk of damage to optics/detectors in the highly unlikely event of a leak. Solution is filled from the bottom with outlets at the highest points in each chamber to enable complete filling and removal of

APPLICATION NOTE
doi.org/10.1002/elsa.202100141
Chemistry Europe
European Chemical Societies Publishing

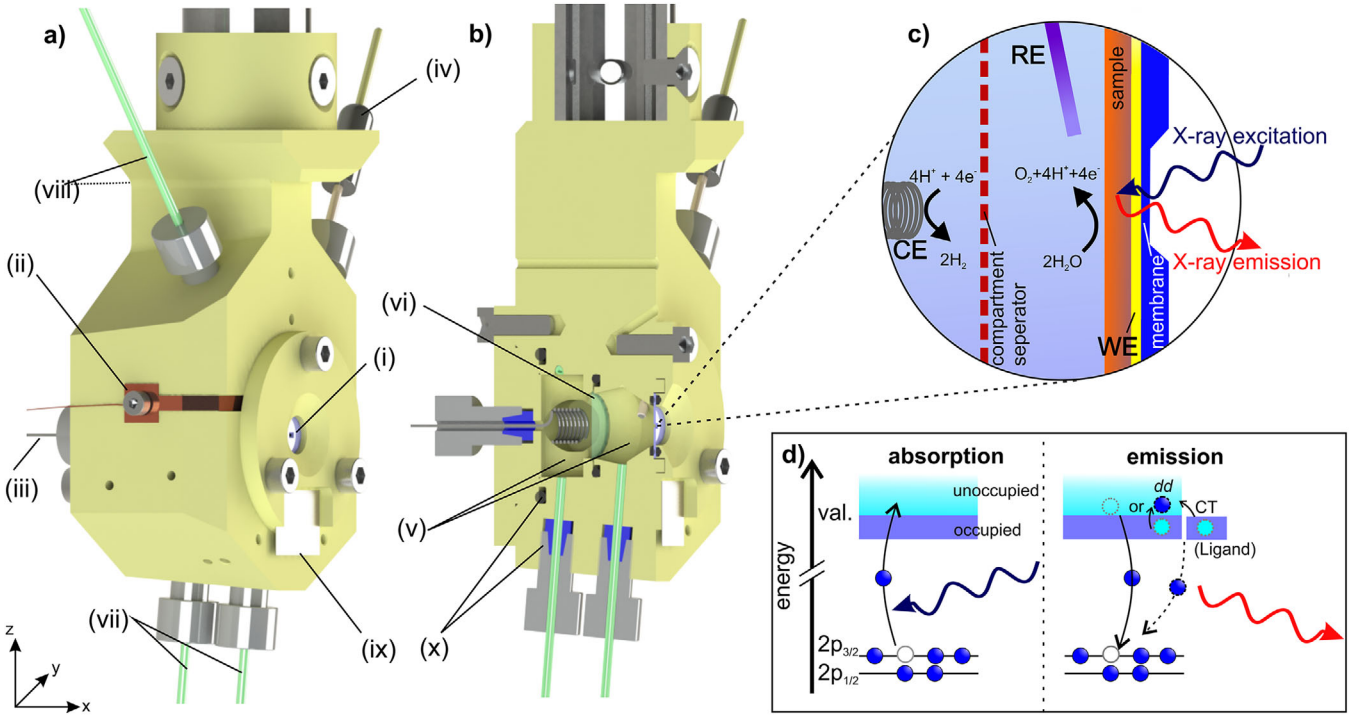

FIGURE 1 3D view (a) and cross-sectional view (b) of the flow cell: The cell consists of a PEEK body comprising a three-electrode setup with (i) working electrode (WE) supported on an X-ray permeable membrane contacted via (ii) a Cu-connector, (iii) a counter electrode (CE) and (iv) a reference electrode (RE). The electrochemical reactions take place in (v) two compartments separated by an (vi) ion-conductive polymer such as Nafion. The compartments can be individually filled via (vii) solution inlet and (viii) outlet ports (second outlet port not visible in 3D-view). For assembly and cleaning, the cell can be opened via back and front lids. The latter is equipped with (ix) a sample mount for reference samples. Lids and connectors are assembled via screws in combination with (x) vacuum-tight sealings. (c) Schematic of the X-ray interaction with the sample through the X-ray permeable membrane and the working electrode during an exemplary electrocatalytic operation, and (d) principle of the X-ray absorption and emission processes

air/gases (Figure 1b). Especially in the case of gas-forming reactions, the conical shape of the WE compartment facilitates gas removal from the electrode and prevents bubble accumulation, which may otherwise isolate areas of the electrode and render them electrochemically inactive. The cylindrical CE compartment provides a surface for immobilizing the compartment separator with Viton O-rings. The use of separate tubing systems for the WE and CE compartments prevents contamination/product-crossover as well as allows the compartments to be drained and refilled independently. Importantly, this design allows solution flow while the cell is installed in a vacuum chamber, thus enabling measurements with convection as well as quiescent conditions. The electrolyte can also be fully exchanged while the cell is under vacuum. The electrolyte in- and outlet tubing as well as the reference and counter electrodes are connected to the flow cell body via vacuum-tight XP-235-screw|P-200-ferrule combinations. For assembly, the counter electrode and the working electrode are attached with PEEK lids to the cell body, sealed with Viton O-rings. This arrangement allows the cell to work in a vacuum environment down to *ca* 5×10^{-7} mbar.

The electrical contacts for the CE, RE, and WE are outside of the cell body, with electrical contact to the WE via a Cu-sheet contacting the edge of the electrode below the lid outside the electrolyte solution. Connection to a potentiostat necessitates electrical feedthrough in the vacuum chamber. The cell is designed for mounting on a 4-axis manipulator (x, y, z, and rotation around z, see Figure 1) for alignment with μm-accuracy in a (typically) 45° angle with respect to the incident beam. The cell design is applicable for any suitable type of spectrometer/endstation, though the mounting points shown are adapted for the LiXEdrom endstation[16] of the synchrotron radiation light source BESSY II, Berlin.

3 | APPLICATION OF SOFT X-RAY PHOTON-IN–PHOTON-OUT SPECTROSCOPY

Soft X-rays cover excitations from $L_{2,3}$-edges ($2p_{3/2}$ and $2p_{1/2}$ core orbitals) of 3*d* transition metals, which are often explored as alternatives to noble metals in electrocatalysis.

APPLICATION NOTE
doi.org/10.1002/elsa.202100141
Chemistry Europe
European Chemical Societies Publishing

They also cover the K-edges (1*s* orbital) of low Z-elements such as C, N, and O, which can be part of energy materials and/or reagents/products of catalytic reactions. For transition metal oxides, the dipole allowed excitations from the metal and oxygen core levels to the hybridized 3*d*-2*p* valence levels are very sensitive to changes in the valence electronic structure, and therefore ideal to study oxidation state changes in the material during operation.

A simplified schematic of the electronic transitions is illustrated in Figure 1d for the $L_{2,3}$-edges, wherein a core level electron is first excited to an unoccupied valence state. The relaxation of this state (electron-hole recombination) can proceed by a fluorescent process emitting a photon of characteristic energy for the final state. Tuning the excitation energy across the core absorption edge energies and measuring the emitted photons gives the fluorescence spectrum (TFY mode), which is similar, however, not identical, to the X-ray absorption spectrum.[17,18] Energy-resolving the emitted photons provides even further information, as is done for X-ray emission spectroscopy (XES) and resonant inelastic X-ray scattering (RIXS; also known as resonant XES). These methods probe occupied electronic states and intra- and interatomic electronic transitions such as *d*-*d* and charger transfer (CT) processes (indicated in Figure 1d).

Herein, we focus on experimental considerations of sample and spectra handling, with the interested reader referred to textbooks and relevant literature for details on the underlying physics of X-ray spectroscopy, for example, references [18–24]. In the following, several considerations about sample and spectra handling are discussed when applying soft X-ray spectroscopy in the presented experimental configuration.

3.1 | X-ray attenuation by membrane and working electrode

Typical dimensions of commercially available X-ray permeable membranes for this application are 0.5 mm × 1.0 mm × 75 nm, inset into a larger frame. These are coated with a conductive layer that functions as the WE, such as a 20 nm Au layer on a 5 nm Ti adhesion layer. The penetration depth of soft X-rays (i.e., photons of *ca* 100–1000 eV) into Si_3N_4 varies from <10 nm at 100 eV to >1000 nm at 1000 eV.[15,25] For a 75 nm thin membrane covered with 5 nm Ti and 20 nm Au, this results in a transmission in normal incidence ranging from *ca* 10% at 100 eV up to *ca* 75% at 1000 eV (Figure 2), clearly rendering spectroscopy on elements with higher excitation energies more feasible. Note that the incident as well as emitted photons need to pass through the membrane and working electrode, though the photon flux for the incident beam can be increased to compensate for the losses without changing the flux on the sample. Naturally, the membrane material and coatings should not contain any elements to be investigated spectroscopically as these would contribute to the observed spectra.

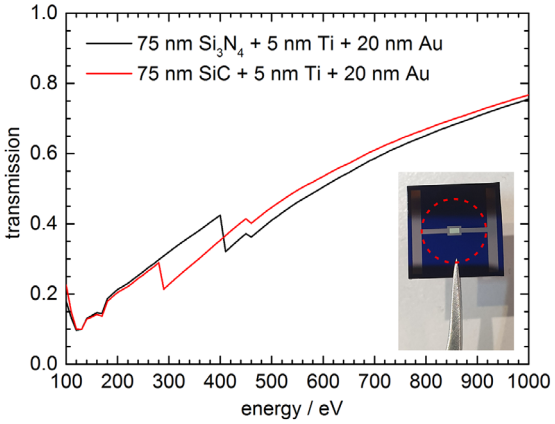

FIGURE 2 Calculated transmission of 75 nm Si_3N_4 and SiC, respectively, each covered with 5 nm Ti and 20 nm Au.[15,25] At *ca* 280, 400, and 450 eV, the edge jumps of carbon, nitrogen, and titanium, respectively, are visible. Inset: Photograph of the Si-frame (held by tweezers), showing the side facing the electrolyte solution with the Au-pattern covering the X-ray permeable membrane (light rectangular area in the center) and providing contact to the Si-frame edges. The red dashed circle indicates the area that is in contact with the electrolyte solution after sealing with an O-ring

3.2 | Balancing the electrochemically and spectroscopically accessible areas

It is prudent to match the electrochemically active surface area to that which is spectroscopically accessible, such as by using a patterned deposition as shown in the inset of Figure 2. This ensures that the electrochemical response is more representative of the area examined spectroscopically and that beam-induced effects are electrochemically detectable. Furthermore, the smaller active area means less bubble formation for gas evolving reactions, an increased ratio of electrolyte volume with respect to the electrode area, and an easier identification of X-ray-induced irregularities/damage in the electrochemical response of the sample. For example, the aforementioned membrane dimensions provide a 0.5 mm^2 area accessible to spectroscopic analysis, while coating the entire Si-frame would give a *ca* 40 mm^2 active area indicated by the red circle in the inset of Figure 2. A patterned Au deposition limits the conductive area in contact with the electrolyte to *ca* 4 mm^2, which covers primarily the membrane area and provides contact to the frame edge for the electrical contact.

doi.org/10.1002/elsa.202100141

3.3 | Sample thickness and morphology

As the sample is probed through the electrode substrate (Figure 1c), the sample has to be thin enough for the X-rays to access the sample|solution interface and to avoid measuring solely buried material.[26] Additionally, the use of thin films reduces self-absorption effects that can cause spectral distortions in fluorescence yield. Experiments on layers with different thickness are useful to disentangle surface and bulk related effects. Note, that although the material contributing to electrochemical reactions is restricted to the surface, the bulk fraction of the sample can also undergo electrochemical transformations.[27] Another approach to increase the surface-related signal is the preparation of porous samples or nanoparticles. Extended discussions on the sample thickness and morphology are provided in Section 3 of the Supporting Information.

3.4 | Measurement sequences and X-ray induced damage

In an ideal in situ spectroelectrochemical experiment, the potential-dependent changes in the spectra demonstrate a reproducible cycling behavior, that is, the material should be adopting a particular state at a given potential irrespective of the sequence of measurements. However, this is not always the case with one example being a sample that requires significant time to reach an equilibrium state. To test this, repeated measurements without changing the conditions, in particular the electrode potential, can be undertaken. Moreover, some of the potential-induced transformations might be irreversible, which might not be immediately obvious at the start of the experiments. Hence, the sequence and duration of the potentials applied during the in situ XAS measurements, including the pretreatment that might be necessary for selected systems, need to be planned on a case-by-case basis.

In addition to the intended potential induced changes, irradiating the sample with X-rays can also transform the material of interest via a combination of mechanisms, often involving photo-induced redox processes, known collectively as radiation (or beam) damage. Commonly, this can be addressed by reducing the flux and/or the irradiation time. It is noted though that soft X-ray photon-out techniques generally require *ca* 100-fold higher X-ray intensity to obtain an emission intensity comparable to that from the electron-out techniques,[28,29] which clearly aggravates the radiation damage problem. To ensure minimal impact of the X-ray-induced effects on the recorded spectroelectrochemical data, control measurements are required prior, during, and after the analysis.

A straightforward procedure to identify the X-ray flux/time that causes spectral changes is to record a series of short spectra, e.g. across the L_3 edge of a transition metal, with sequentially increasing X-ray flux for each subsequent spectrum to identify the highest irradiation intensity/time that does not induce detectable spectral changes. This procedure should be applied for all conditions (potentials) of interest, since different states of an electromaterial are likely to be impacted by X-rays in a different manner and to a different extent.[26] The lowest possible flux that offers a reasonable signal-to-noise ratio without damaging the sample should then be used for all measurements to facilitate comparisons of the data. To further ensure reproducibility of the data, measurements on one spot/area should be repeated at least twice, and at least one additional scan should be collected on a pristine spot/area under identical measurement conditions.

To reduce the flux density while maintaining the signal intensity for TFY and PFY experiments, the size of the beam spot on the sample can be increased. However, a small beam spot is necessary to maintain the energy resolution on the detector for XES and RIXS, as typically is a high flux to compensate for the losses when energy resolving the emitted photons (these losses also affect PFY). Under these circumstances, the often unavoidable radiation damage can be suppressed via decreasing the X-ray exposure time by continuously moving the sample during the measurement. After performing XES or RIXS analysis, additional TFY spectra should be recorded on the irradiated area and compared to the initial spectra as an additional check for the radiation damage. Microscopic (visible light or electron) analysis post spectroelectrochemical studies can further assist with the identification of the X-ray-induced changes to the sample.

A detailed scheme of the suggested measurement sequence and an example of radiation-induced damage are provided in Section 4 of the Supporting Information.

3.5 | Interpretation of TFY spectra

It is important to note the differences between pure absorption, electron-yield, and fluorescence-yield spectra. The stronger state dependence of fluorescence decay[20] means it does not necessarily result in pure absorption spectra,[18] especially at the $L_{2,3}$-edges of 3*d*-transition metals.[17] Electron-yield spectra are generally closer to absorption spectra, so care must be taken in comparisons. Additional effects such as self-absorption may also lead to further distortions in TFY analyses.[24] By only detecting emitted photons in a selected energy range, PFY can avoid/reduce these distortions,[20,30,31] though this usually requires higher X-ray intensities than TFY.

APPLICATION NOTE
doi.org/10.1002/elsa.202100141
Chemistry Europe
European Chemical Societies Publishing

Taking these characteristics of TFY spectroscopy into account, qualitative as well as quantitative analysis can be performed, similar to other spectroscopic techniques. Qualitative and semi-quantitative fingerprint analysis is quite effective for the identification of the potential-induced changes within the material. Precise quantitative spectra interpretation typically requires theoretical calculations. These can take the form of configuration interaction, density functional theory, and/or coupled cluster ab initio approaches depending on the system.

3.6 | Applications and challenges

The presented cell is predominately designed for sample configurations in which a material is directly deposited onto the electrode support and is in contact with a liquid electrolyte, enabling studies of a variety of systems.

Soft X-ray photon-in–photon-out spectroelectrochemical analysis, using a prototype of the cell presented herein, was previously conducted to study MnO_x water electrooxidation catalyst[32] as well as potential-induced oxidation behavior of MXenes.[33] The cell design enables studies on the cathode and anode materials and on half-reactions, such as investigated in standard three-electrode laboratory setups. The cell also fulfills the requirements for in situ/*operando* studies on individual battery materials.[34–36] Relatively large volume of the working compartment and its physical separation from the counter electrode excludes interference from the latter and the possibility for short-circuiting failure due to electrodeposition of excessive amounts of the material or its electrochemically-induced expansion. The UV-vis transparency of the WE substrate allows also for studies on photo(electro)active materials. However, the application is restricted to PFY, XES, and RIXS analysis because the additional light source will interfere with the TFY.

The scope of applications covers the tracking of oxidation states during electrochemical cycling, analysis of dissolution or intercalation/deposition of certain elements, probing the reversibility of processes, as well as investigation of potential-induced electronic structure changes and electronic interactions. Most importantly all studies can be conducted on an element selective level.

4 | DEMONSTRATION OF IN SITU TFY ANALYSIS OF AN ELECTRODEPOSITED NiO_x CATALYST

A TFY study on a NiO_x oxygen evolution catalyst electrodeposited in situ as a thin film is presented below to demonstrate the capability of the cell and approach. Note

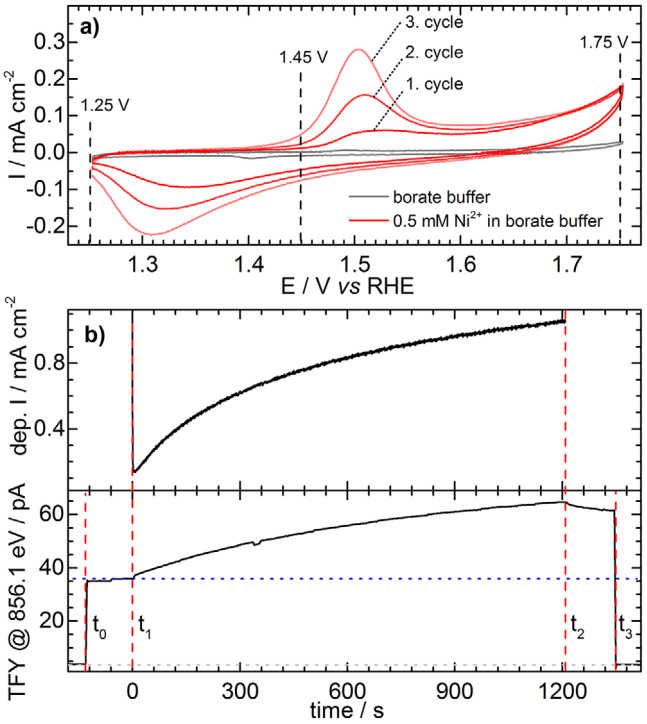

FIGURE 3 (a) Cyclic voltammogram (0.100 V/s) of a bare $Au/Ti/Si_3N_4$ substrate in 0.1 M borate buffer with pH 9.2 (grey), and three repetitive scans after exchanging the solution with the same borate buffer solution containing 0.5 mM Ni^{2+}. (b) Evolution of the deposition current density (top) and simultaneously collected TFY signal (bottom) at the Ni resonance at 856.1 eV during NiO_x deposition at 1.75 V vs. RHE (see text for further details)

that further experiment types such as PFY, XES, and RIXS are applicable with the setup, however, are more challenging with respect to avoiding radiation damage (see above and Section 4 in the Supporting Information). An example of PFY/RIXS experiments conducted with a prototype of the cell presented herein can be found elsewhere.[32]

4.1 | In situ sample preparation

Electrochemical testing and deposition were done while the electrochemical cell was within the spectroscopy chamber and under vacuum. Experimental details are provided in Section 1 of the Supporting Information. Prior to sample deposition, cyclic voltammetry of the bare Au-coated Si_3N_4 substrate in borate buffer (0.1 M, pH 9.2) shows the expected electrochemical response of a gold electrode (Figure 3a). After the exchange with the 0.5 mM Ni^{2+} solution in the same borate buffer, voltammetry exhibits an oxidation peak at *ca* 1.5 V_{RHE} and a reduction peak at *ca* 1.3 V_{RHE}, which increases in intensity with subsequent scans as is indicative of the oxidative electrodeposition of a NiO_x film. Chronoamperometry at

doi.org/10.1002/elsa.202100141

1.75 V_{RHE} with gentle solution flow was then employed to deposit a film of a suitable thickness. Since the film is catalytically active at the deposition potential, the observed current results from water oxidation and film formation. To optimize the catalyst film thickness for X-ray examination, the TFY signal at a known Ni resonance (the Ni L_3-edge at 856.1 eV) was recorded simultaneously to the deposition (Figure 3b).

Opening the beamshutter (t_0) and allowing X-rays to irradiate the WE, increases the signal on the diode from the dark current (dashed gray line in Figure 3b) to a background signal caused by non-resonant fluorescence (dashed blue line in Figure 3b). Chronoamperometry was performed between points t_1 and t_2, leading to a steady increase of the TFY signal due to film growth. After the deposition stops, the TFY signal showed a slight decrease, which can originate from either partial material loss or change in Ni oxidation state without applied potential. At t_3 the beamshutter was closed. Importantly, the TFY signal was not saturated during electrodeposition, verifying that at all times the film was thin enough for the X-ray to access freshly deposited material, and thereby the interface with the solution. After deposition, the solution was exchanged with the precursor-free solution for the subsequent analysis.

4.2 | X-ray absorption spectroscopy in total fluorescence yield

One centerpiece of in situ/*operando* soft X-ray analysis is the measurement of absorption spectra to obtain information of changes occurring in the (electronic) structure of the material. To this end, measuring the TFY is a powerful approach to track the material's electronic structure under operative conditions. The Ni L-edge TFY spectrum at 1.25 V_{RHE} exhibits pronounced peaks at 853.7 eV and 855.7 eV, with the shape resembling spectra of Ni in a 2+ oxidation state.[37] Increasing the potential to the onset of the Ni oxidation feature at 1.45 V_{RHE} and then to 1.75 V_{RHE} (Figure 4a) results in the first peak at 853.7 eV significantly decreasing in intensity. Concurrently, the peak at 855.7 eV increases in intensity and shifts 0.4 eV to higher energy. Further increasing the potential to 1.90 V_{RHE} where the OER current is extensive does not induce further spectral changes, indicating the sample does not undergo further oxidative transformations. A similar spectral shape can be found for γ-NiOOH[38] though Ni^{4+} also exhibits a prominent feature *ca* 3 eV above the Ni^{2+} main peak.[37] The bulk sensitivity of TFY means the extensive spectral changes are due to changes of the complete or at least a large fraction of the sample, and not only of a surface layer. Bulk oxidation with the formation of a NiOOH phase under alkaline

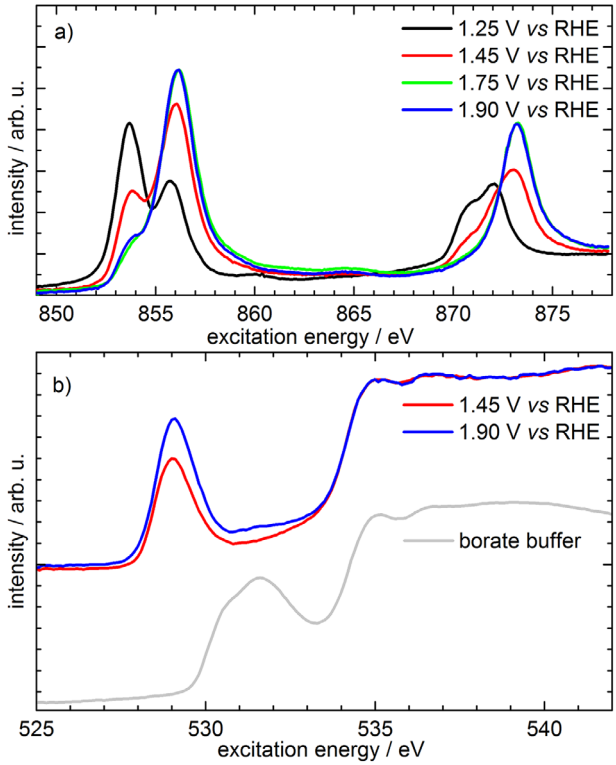

FIGURE 4 TFY spectra collected at selected potentials across the (a) Ni $L_{2,3}$-edges and (b) the O K-edge. To identify contributions in the O K-edge spectra not stemming from the catalyst film, a spectrum taken on 0.1 M borate buffer behind an Au/Ti-coated Si_3N_4 membrane(light grey), is shown for comparison

conditions is in agreement with published reports.[27] Bulk oxidation has also been observed previously for thin Mn[32] and Co[39,40] oxyhydroxide catalyst films.

In contrast to hard X-ray studies, soft X-ray analysis facilitates complementary measurements at the O K-edge. Note, that all oxygen-containing components contribute to these spectra. A reference spectrum of a borate buffer electrolyte shows a broad pre-edge feature from *ca* 530-533 eV (Figure 4b), and an edge starting at *ca* 534 eV, where contributions of O in H_2O are dominant.[41] For the latter, X-ray self-absorption can lead to damping of spectral features and signal saturation. The NiO_x film displays a prominent pre-edge peak at 529.0 eV, which increases in intensity when the potential is increased from 1.45 to 1.90 V_{RHE}. Specifically, the pre-edge region of metal oxide O K-edge spectra contains information about oxidation states and phases,[42] metal-oxygen hybridization,[32] and formation of surface oxygen species.[43] This peak originates from transitions from the O1*s* into O 2*p* – Ni 3*d* hybridized states, which are typical transitions observed in all 3*d* transition metal oxides.[44] In a previous study on a manganese oxide electrocatalyst, the intensity change of the metal pre-peak could be related to changes in orbital hybridization as the potential was increased towards more positive values.[32]

APPLICATION NOTE
doi.org/10.1002/elsa.202100141
Chemistry Europe
European Chemical Societies Publishing

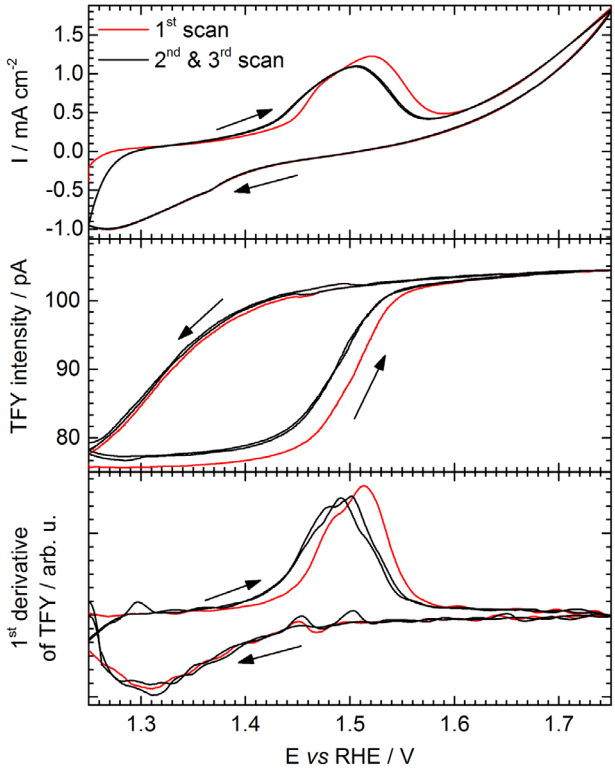

FIGURE 5 Dynamic analysis of the redox behavior of the NiO_x electrocatalyst. Redox features in cyclic voltammetry at 0.005 V/s (top panel) are directly reflected in the change of the TFY signal (middle panel) at 856.1 eV. The derivative of the TFY signal yields an element selective redox curve (bottom panel). Arrows show the sweep direction

4.3 | Fluorescence yield detection during voltammetry

Measuring the fluorescence yield at a fixed energy during cyclic voltammetry allows electrochemically observed redox processes to be directly assigned to spectral changes at the selected energy. Crucially, it provides an element selective picture of the redox behavior of the sample. This method was first implemented for hard X-rays under the term fixed energy X-ray absorption voltammetry (FEXRAV),[45] though only a few groups have reported its application.[46–49]

Fixing the excitation X-ray energy at 856.1 eV and measuring the TFY response allows changes in the oxidized Ni state to be related to the voltammetric response. Three voltammetric cycles were measured between 1.25 V_{RHE} and 1.75 V_{RHE}, with the first scan deviating slightly from the subsequent scans as is normally the case (top panel in Figure 5). The TFY signal at 856.1 eV exhibits an increase at ~1.5 V_{RHE} on the forward scan and a subsequent decrease in the reverse scan at ~1.35 V_{RHE} (middle panel in Figure 5). This increase/decrease of the TFY originates in the previously discussed change of the TFY spectra for Ni in different oxidation states (Figure 4a). To interpret the results and connect them to oxidation state changes, the derivative of the TFY signal can be plotted against the applied potential (bottom panel of Figure 5). The TFY signal was smoothed to remove noise in the derivative using a second-degree polynomial Savitzki-Golay-filter in a 50-point window (corresponding to 0.025 V). Importantly, the redox features of the voltammetric scans are perfectly reproduced by the derivative of the TFY signal, including the aforementioned shift of the first voltammetric scan. Moreover, the OER current manifesting in voltammograms is absent in the derivative of the TFY because it is not related to a detectable change in the Ni oxidation state. This strikingly illustrates the strength of the method to disentangle different redox processes by creating an element selective redox curve. This is especially valuable for processes that might be obscured by reaction currents in electrochemical data or for the element selective analysis of multi-element systems and allow redox processes to be spectroscopically assigned to specific oxidation state changes.

5 | CONCLUSION AND OUTLOOK

This work presents an overview of the application of soft X-ray photon-in–photon-out spectroscopy to energy materials and an electrochemistry flow cell designed for high-quality measurements. Typical experimental parameters of the cell as well the spectroscopic setup are given in Table 1. The cell provides advantageous electrochemical conditions such as separated electrolyte compartments with volumes each > 1 mL and the option for an in situ sample deposition and full electrochemical (pre)treatment of the sample before and during X-ray spectroscopic analysis. Several important aspects of sample and spectra handling were discussed and the applicability of X-ray absorption and emission spectroscopy was demonstrated on an in situ electrodeposited NiO_x catalyst film for the OER. Crucially, the cell produced an excellent voltammetric response and allowed TFY to track the film electrodeposition. It also enabled potential-dependent changes to TFY spectra to be observed at the Ni $L_{2,3}$-edges, showing oxidation state changes in the film under electrocatalytic operating conditions. It was further shown that the high sensitivity and voltammetric response allows fixed energy TFY measurements to monitor redox changes during voltammetry, and prepare an element selective redox curve.

Overall it was shown that in situ/*operando* soft X-ray photon-in–photon-out spectroscopy is a powerful tool to

TABLE 1 Overview of flow cell parameters and experimental conditions for application in the LiXEdrom endstation at U49-2 PGM-1 at BESSY II

Cell parameters		**Experimental parameters**	
Electrolyte volume:	*ca* 1 mL WE compartment *ca* 2 mL CE compartment	Min./max. vacuum	5×10^{-5}- 5×10^{-7}
Flow rate	Variable. Typical range: 1 - 50 μL s^{-1}	Energy range	*ca* 200 - 1200 eV
Membrane materials	Si_3N_4, SiC, Si	Detector (TFY)	XUV-100 silicon photodiode
Frame dimensions	10 mm × 10 mm × 0.381 mm	Energy resolution (TYF/PFY)	Dependent on beamline settings. Typical: 100 meV
Membrane size	Variable. Typical: 1 mm × 0.5 mm × 100 nm	Detector (PFY/XES/RIXS)	MCP|fluorescence screen|CCD stack
Standard coating	5 nm Ti adhesion layer 20 nm Au conductive support	Energy resolution (RIXS/XES)	Typical: $\Delta E/E > 500$
Reference electrode	Ag|AgCl in 3.4 M KCl	Beam size (ver. x hor.)	Variable: from 20 μm × 80 μm to 100 μm × 100 μm
Counter electrode	Exchangeable. Standard: Pt-Wire	Accuracy of beam positioning	*ca* 1 μm
Compartment separator	Ion-selective polymer (e.g. Nafion) or a separator (e.g. Zirfon)	Temperature	Room temperature

study potential induced changes in energy materials, highlighting the importance to investigate a material designed for electrochemical purposes under operative conditions. Its high sensitivity to changes in the 3*d*-valence structure of transition metals and the option to perform additional experiments at C, N and O K-edges renders it a versatile and highly informative spectroscopic technique.

ACKNOWLEDGMENTS

MFT, ANS, and RS acknowledge financial support by the German Federal Ministry of Education and Research (BMBF project "PrometH_2eus", FKZ 03HY105E). SAB gratefully acknowledges an Alexander von Humboldt Postdoctoral Fellowship. ANS acknowledges financial support from the Australian Research Council (Centre of Excellence for Electromaterials Science CE140100012, Future Fellowship Grant FT200100317). Measurements were carried out at the U49-2 PGM-1 beamline and LiXEdrom endstation at the BESSY II electron storage ring operated by the Helmholtz-Zentrum Berlin für Materialien und Energie.

CONFLICT OF INTEREST

The authors declare no conflict of interest.

DATA AVAILABILITY STATEMENT

The data that support the findings of this study are available from the corresponding author upon reasonable request.

ORCID

Marc F. Tesch https://orcid.org/0000-0001-7480-7200
Alexandr N. Simonov https://orcid.org/0000-0003-3063-6539

REFERENCES

1. S. W. Chee, T. Lunkenbein, R. Schlögl, B. R. Cuenya, *J. Phys.: Condens. Matter* **2021**, *33*, 153001.
2. G. Rupprechter, *Small* **2021**, *17*, 2004289.
3. O. Panchenko, M. Carmo, M. Rasinski, T. Arlt, I. Manke, M. Müller, W. Lehnert, *Materials Today Energy* **2020**, *16*, 100394.
4. S. A. Bonke, T. Risse, A. Schnegg, A. Brückner, *Nat Rev Methods Primers* **2021**, *1*, 1.
5. C. H. M. van Oversteeg, H. Q. Doan, F. M. F. de Groot, T. Cuk, *Chem. Soc. Rev.* **2017**, *46*, 102.
6. J. Timoshenko, B. Roldan Cuenya, *Chem. Rev.* **2021**, *121*, 882.
7. D. Liu, Z. Shadike, R. Lin, K. Qian, H. Li, K. Li, S. Wang, Q. Yu, M. Liu, S. Ganapathy, X. Qin, Q.-H. Yang, M. Wagemaker, F. Kang, X.-Q. Yang, B. Li, *Adv. Mater.* **2019**, *31*, 1806620.
8. A. Kolmakov, D. A. Dikin, L. J. Cote, J. Huang, M. K. Abyaneh, M. Amati, L. Gregoratti, S. Günther, M. Kiskinova, *Nature Nanotech* **2011**, *6*, 651.
9. J. J. Velasco-Velez, V. Pfeifer, M. Hävecker, R. S. Weatherup, R. Arrigo, C.-H. Chuang, E. Stotz, G. Weinberg, M. Salmeron, R. Schlögl, A. Knop-Gericke, *Angew. Chem., Int. Ed.* **2015**, *54*, 14554.
10. P. Jiang, J.-L. Chen, F. Borondics, P.-A. Glans, M. W. West, C.-L. Chang, M. Salmeron, J. Guo, *Electrochem. Commun.* **2010**, *12*, 820.
11. J.-J. Velasco-Velez, C. H. Wu, T. A. Pascal, L. F. Wan, J. Guo, D. Prendergast, M. Salmeron, *Science* **2014**, *346*, 831.
12. C. Schwanke, R. Golnak, J. Xiao, K. M. Lange, *Rev. Sci. Instrum.* **2014**, *85*, 103120.

13. D. K. Bora, P.-A. Glans, J. Pepper, Y.-S. Liu, C. Du, D. Wang, J.-H. Guo, *Rev. Sci. Instrum.* **2014**, *85*, 043106.
14. T. Ishihara, T. Tokushima, Y. Horikawa, M. Kato, I. Yagi, *Rev. Sci. Instrum.* **2017**, *88*, 104101.
15. B. L. Henke, E. M. Gullikson, J. C. Davis, *Atomic Data and Nuclear Data Tables* **1993**, *54*, 181.
16. Helmholtz-Zentrum Berlin für Materialien und Energie, *Journal of large-scale research facilities* **2016**, *2*, A80.
17. R. Kurian, K. Kunnus, P. Wernet, S. M. Butorin, P. Glatzel, F. M. F. de Groot, *J. Phys.: Condens. Matter* **2012**, *24*, 452201.
18. F. M. F. de Groot, M. A. Arrio, Ph. Sainctavit, Ch. Cartier, C. T. Chen, *Solid State Commun.* **1994**, *92*, 991.
19. L. J. P. Ament, M. van Veenendaal, T. P. Devereaux, J. P. Hill, J. van den Brink, *Rev. Mod. Phys.* **2011**, *83*, 705.
20. R. Golnak, J. Xiao, K. Atak, I. Unger, R. Seidel, B. Winter, E. F. Aziz, *The Journal of Physical Chemistry A* **2016**, *120*, 2808.
21. R. Golnak, S. I. Bokarev, R. Seidel, J. Xiao, G. Grell, K. Atak, I. Unger, S. Thürmer, S. G. Aziz, O. Kühn, B. Winter, E. F. Aziz, *Sci. Rep.* **2016**, *6*, 24659.
22. F. de Groot, A. Kotani, *Core Level Spectroscopy of Solids*, CRC Press, Boca Raton **2008**.
23. Y.-S. Liu, P.-A. Glans, C.-H. Chuang, M. Kapilashrami, J. Guo, *J. Electron Spectrosc. Relat. Phenom.* **2015**, *200*, 282.
24. S. Eisebitt, T. Böske, J.-E. Rubensson, W. Eberhardt, *Phys. Rev. B* **1993**, *47*, 14103.
25. "CXRO X-Ray Interactions with Matter," can be found under https://henke.lbl.gov/optical_constants/
26. H. J. King, M. Fournier, S. A. Bonke, E. Seeman, M. Chatti, A. N. Jumabekov, B. Johannessen, P. Kappen, A. N. Simonov, R. K. Hocking, *J. Phys. Chem. C* **2019**, *123*, 28533.
27. S. Corby, M.-G. Tecedor, S. Tengeler, C. Steinert, B. Moss, C. A. Mesa, H. F. Heiba, A. A. Wilson, B. Kaiser, W. Jaegermann, L. Francàs, S. Gimenez, J. R. Durrant, *Sustainable Energy Fuels* **2020**, *4*, 5024.
28. M. O. Krause, *J. Phys. Chem. Ref. Data* **1979**, *8*, 307.
29. A. Kotani, S. Shin, *Rev. Mod. Phys.* **2001**, *73*, 203.
30. A. J. Achkar, T. Z. Regier, H. Wadati, Y.-J. Kim, H. Zhang, D. G. Hawthorn, *Phys. Rev. B* **2011**, *83*, 081106.
31. W. Yang, T. P. Devereaux, *J. Power Sources* **2018**, *389*, 188.
32. M. F. Tesch, S. A. Bonke, T. E. Jones, M. N. Shaker, J. Xiao, K. Skorupska, R. Mom, J. Melder, P. Kurz, A. Knop-Gericke, R. Schlögl, R. K. Hocking, A. N. Simonov, *Angew. Chem., Int. Ed.* **2019**, *58*, 3426.
33. A. Al-Temimy, K. Prenger, R. Golnak, M. Lounasvuori, M. Naguib, T. Petit, *ACS Appl. Mater. Interfaces* **2020**, *12*, 15087.
34. F. Yang, X. Feng, Y.-S. Liu, L. C. Kao, P.-A. Glans, W. Yang, J. Guo, *Energy & Environmental Materials* **2021**, *4*, 139.
35. K. Yamanaka, K. Nakanishi, I. Watanabe, T. Ohta, *Electrochemistry* **2018**, *86*, 128.
36. P. Ghigna, E. Quartarone, *J. Phys. Energy* **2021**, *3*, 032006.
37. X. Zheng, B. Zhang, P. De Luna, Y. Liang, R. Comin, O. Voznyy, L. Han, F. P. García de Arquer, M. Liu, C. T. Dinh, T. Regier, J. J. Dynes, S. He, H. L. Xin, H. Peng, D. Prendergast, X. Du, E. H. Sargent, *Nat. Chem.* **2018**, *10*, 149.
38. M. Al Samarai, A. W. Hahn, A. Beheshti Askari, Y.-T. Cui, K. Yamazoe, J. Miyawaki, Y. Harada, O. Rüdiger, S. DeBeer, *ACS Appl. Mater. Interfaces* **2019**, *11*, 38595.
39. J. Zhou, Y. Wang, X. Su, S. Gu, R. Liu, Y. Huang, S. Yan, J. Li, S. Zhang, *Energy Environ. Sci.* **2019**, *12*, 739.
40. M. W. Kanan, J. Yano, Y. Surendranath, M. Dincă, V. K. Yachandra, D. G. Nocera, *J. Am. Chem. Soc.* **2010**, *132*, 13692.
41. L.-A. Näslund, J. Lüning, Y. Ufuktepe, H. Ogasawara, P. Wernet, U. Bergmann, L. G. M. Pettersson, A. Nilsson, *J. Phys. Chem. B* **2005**, *109*, 13835.
42. M. N. Shaker, S. A. Bonke, J. Xiao, M. A. Khan, R. K. Hocking, M. F. Tesch, *ChemPlusChem* **2018**, *83*, 721.
43. V. Pfeifer, T. E. Jones, J. J. V. Vélez, R. Arrigo, S. Piccinin, M. Hävecker, A. Knop-Gericke, R. Schlögl, *Chem. Sci.* **2017**, *8*, 2143.
44. F. M. F. de Groot, J. C. Fuggle, B. T. Thole, G. A. Sawatzky, *Phys. Rev. B* **1990**, *42*, 5459.
45. A. Minguzzi, O. Lugaresi, C. Locatelli, S. Rondinini, F. D'Acapito, E. Achilli, P. Ghigna, *Anal. Chem.* **2013**, *85*, 7009.
46. M. Fracchia, P. Ghigna, A. Vertova, S. Rondinini, A. Minguzzi, *Surfaces* **2018**, *1*, 138.
47. E. Berretti, A. Giaccherini, G. Montegrossi, F. D'Acapito, F. Di Benedetto, C. Zafferoni, A. Puri, G. O. Lepore, H. Miller, W. Giurlani, M. Innocenti, F. Vizza, A. Lavacchi, *Catalysts* **2019**, *9*, 659.
48. D. Drevon, M. Görlin, P. Chernev, L. Xi, H. Dau, K. M. Lange, *Sci. Rep.* **2019**, *9*, 1532.
49. D. González-Flores, K. Klingan, P. Chernev, S. Loos, M. Reza Mohammadi, C. Pasquini, P. Kubella, I. Zaharieva, R. D. L. Smith, H. Dau, *Sustainable Energy Fuels* **2018**, *2*, 1986.

SUPPORTING INFORMATION

Additional supporting information may be found in the online version of the article at the publisher's website.

How to cite this article: M. F. Tesch, S. A. Bonke, R. Golnak, J. Xiao, A. N. Simonov, R. Schlögl, *Electrochem Sci Adv* **2021**, e2100141. https://doi.org/10.1002/elsa.202100141